Please cite this article in press as: Antzoulatos and Miller, Increases in Functional Connectivity between Prefrontal Cortex and Striatum during Category Learning, Neuron (2014), http://dx.doi.org/10.1016/j.neuron.2014.05.005

Neuron
Article

Increases in Functional Connectivity between Prefrontal Cortex and Striatum during Category Learning

Evan G. Antzoulatos[1,2,*] and Earl K. Miller[1,*]
[1]The Picower Institute for Learning & Memory, Department of Brain & Cognitive Sciences, Massachusetts Institute of Technology, Cambridge, MA 02139, USA
[2]Center for Neuroscience, Department of Neurobiology, Physiology and Behavior, University of California, Davis, Davis, CA 95618, USA
*Correspondence: eantzoulatos@ucdavis.edu (E.G.A.), ekmiller@mit.edu (E.K.M.)
http://dx.doi.org/10.1016/j.neuron.2014.05.005

SUMMARY

Functional connectivity between the prefrontal cortex (PFC) and striatum (STR) is thought critical for cognition and has been linked to conditions like autism and schizophrenia. We recorded from multiple electrodes in PFC and STR while monkeys acquired new categories. Category learning was accompanied by an increase in beta band synchronization of LFPs between, but not within, the PFC and STR. After learning, different pairs of PFC-STR electrodes showed stronger synchrony for one or the other category, suggesting category-specific functional circuits. This category-specific synchrony was also seen between PFC spikes and STR LFPs, but not the reverse, reflecting the direct monosynaptic connections from the PFC to STR. However, causal connectivity analyses suggested that the polysynaptic connections from STR to the PFC exerted a stronger overall influence. This supports models positing that the basal ganglia "train" the PFC. Category learning may depend on the formation of functional circuits between the PFC and STR.

INTRODUCTION

Anatomical loops between the prefrontal cortex (PFC) and basal ganglia (BG) suggest a close functional relationship, but the nature of their interactions is not yet understood. It is clear that both areas are critical for learning. One hypothesis is that they have different types of plasticity: The BG (in particular the striatum or STR) are thought to rapidly acquire simple information (single associations, decision alternatives, etc.) in piecemeal fashion, while the PFC knits together such details into more elaborate and generalized representations (Daw et al., 2005). Interactions between these mechanisms may explain category learning (Seger and Miller, 2010). The idea is that the STR rapidly forms associations that are then fed through the BG to the PFC (Ashby et al., 2007; Djurfeldt et al., 2001). Iterations allow more gradual changes in synaptic weights in the PFC to detect and store the common features across patterns learned by the BG, thereby acquiring the categories (Miller and Buschman, 2008; Seger and Miller, 2010).

Support for this comes from human imaging studies showing that both the PFC and STR are engaged during category learning (Reber et al., 1998; Seger et al., 2000; Vogels et al., 2002). Also, computational and neurophysiological studies suggest more rapid changes in the STR than PFC during learning, as if the BG was "training" the cortex (Djurfeldt et al., 2001; Pasupathy and Miller, 2005). We recently provided more direct support in monkeys trained to learn new categories (Antzoulatos and Miller, 2011). There was the predicted reversal: Early in learning, when the associations of a few stimuli could be formed, the STR led; its activity was the earliest predictor of the behavioral choice. But then, as the animals began to truly acquire categories, the PFC became the earliest predictor of the choice.

While such results are certainly suggestive of PFC-BG functional interactions, direct evidence for functional interactions between the PFC and STR is rare. It is possible that these structures are part of different learning systems that work relatively independently. We sought to test for functional connectivity between the PFC and STR by examining synchrony between oscillations of their local field potentials (LFPs) (Friston et al., 2013). Frequency-dependent synchrony between LFPs suggests neural communication and has been observed in perceptual (Hipp et al., 2011), motor (Brovelli et al., 2004), and cognitive tasks (Daitch et al., 2013). The functional connectivity between BG and PFC is of particular interest, as the network between them has been implicated in several neurological and psychiatric conditions, such as autism and schizophrenia (Padmanabhan et al., 2013; Uhlhaas and Singer, 2012; Yoon et al., 2013). We found evidence that functional connectivity between the PFC and STR increased as animals acquired new categories.

RESULTS

Learning-Related Enhancement of Synchrony between the PFC and STR

The animals were required to respond to a randomly chosen category exemplar with a saccade to the left or right target (Figure 1A). All exemplars were created de novo each day through distortion of a new pair of prototypes (Figure 1B). Each training session began with a single new exemplar per category, which monkeys learned as specific stimulus-response (SR)

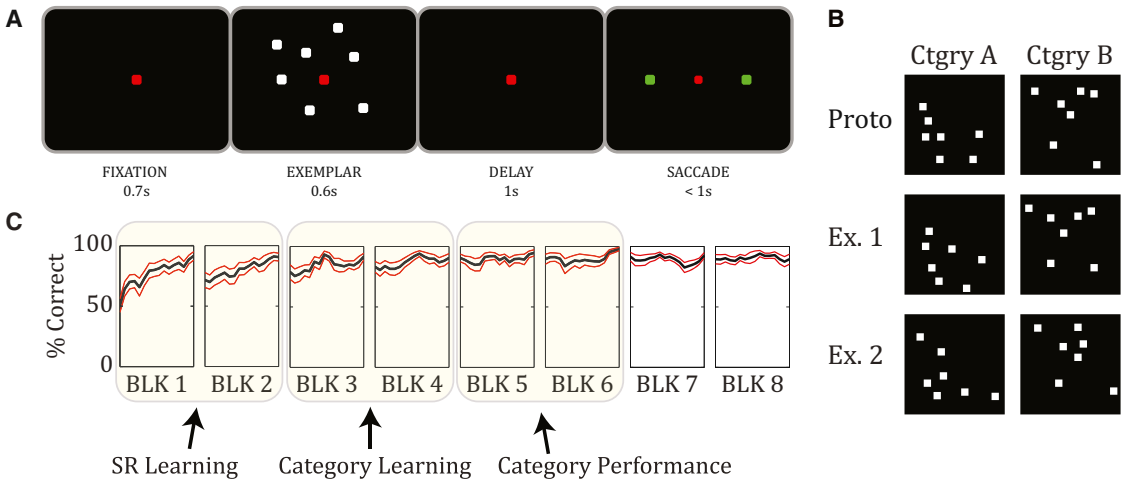

Figure 1. Task Design

(A) The schematic illustrates the time course of a single trial. The animal had to respond to a randomly presented exemplar by choosing between a saccade to the right or left targets (green squares).

(B) Two example categories. New pairs of prototypes (top) were constructed for each recording session. Distortion of each prototype gave rise to hundreds of unique exemplars (only two of which are shown for each category).

(C) Average behavioral performance (% correct) ±SEM across recording sessions. The animals started by learning a few individual SR associations (SR Learning stage: always the first two blocks). As they progressed through the blocks, they were trained on more and more exemplars (Category Learning stage) until they eventually learned the categories and their behavior stabilized (Category Performance stage). The Category Learning and Category Performance stages are shown for illustration only: the timing of each could vary across recording sessions, based on the animals' performance on each new set of categories. (Adapted from Antzoulatos and Miller, 2011.)

associations (Antzoulatos and Miller, 2011). Then, as learning progressed, more and more exemplars were added. This required animals to learn the categories (or fail), because sooner or later, they would be confronted with too many new exemplars to sustain performance by SR learning alone.

Based on the monkeys' performance, we could distinguish three stages of learning (Antzoulatos and Miller, 2011) (Figure 1C). In stage 1 (SR Learning), monkeys learned the category of (i.e., the correct saccade for) each new exemplar individually. In stage 2 (Category Learning), the monkeys were challenged with many more exemplars but began to perform above chance with new exemplars. This indicates the start of acquisition of category information. In stage 3 (Category Performance), learning of the categories was complete. Behavior remained at asymptote even though monkeys were mainly seeing new exemplars for the first time on most trials. We examined changes in synchrony between the PFC and STR as a function of learning stage.

We first calculated synchrony of LFPs between recording sites in the PFC and STR (n = 426 electrode pairs). Each site's LFP signal was decomposed to its frequency components using wavelet analysis (Torrence and Compo, 1998) and then a phase-locking value (PLV) was determined for each pair of simultaneously recorded LFPs (Lachaux et al., 1999). We subtracted out any phase-locking due to external events (e.g., stimulus onset) so that we could isolate true neural synchrony (i.e., the PLV values shown are the difference between observed PLV and surrogate-data PLV) (see Supplemental Experimental Procedures available online). Analysis was focused on two critical task epochs, the last 500 ms of the 600-ms-long exemplar presentation (exemplar epoch) and the last 500 ms preceding the behavioral response (decision epoch). Similar results were obtained from other trial epochs and using diverse measures of synchrony (i.e., coherence and pairwise phase consistency). We first limited this analysis to correctly performed trials; error trials will be considered further below.

This analysis revealed a peak of PFC-STR synchrony in the beta band (defined as 12–30 Hz) during the exemplar and decision epochs (peak at ~20 Hz) (see Figure 2A). After the switch from SR Learning to Category Learning (Stage 1 to 2), there was a significant increase in decision-epoch average beta band PLV between the PFC and STR (Figure 2A, right) (ANOVA, $F(2,1277) = 11.23$, $p = 1.5 \times 10^{-5}$; post hoc comparison: SR Learning PLV less than Category Learning and Category Performance PLV, $p = 0.0005$). Correspondingly, during the decision epoch, there was a learning-related increase in the percentage of pairs of PFC-STR recording sites that showed significant beta band PLV (greater than the 95th percentile of the PLV expected by chance): more pairs showed significant PLV during Category Learning (57.3%, Stage 2) and Category Performance (55.9%, Stage 3) than during SR Learning (42.3%, Stage 1; $p = 0.003$, chi-square test). Learning-related changes in PFC-STR synchrony were limited to the decision epoch. The PFC-STR beta PLV during the exemplar epoch did not significantly increase across learning stages (Figure 2A, left) (ANOVA across stages: $F(2,1277) = 1.06$, $p = 0.35$). Likewise, the number of pairs of PFC-STR recording sites with significant PLV was not different across learning stages for the exemplar epoch (SR Learning: 48.6%; Category Learning: 55.9%; Category Performance: 50.5%; $p = 0.31$, chi-square test). There were also no significant

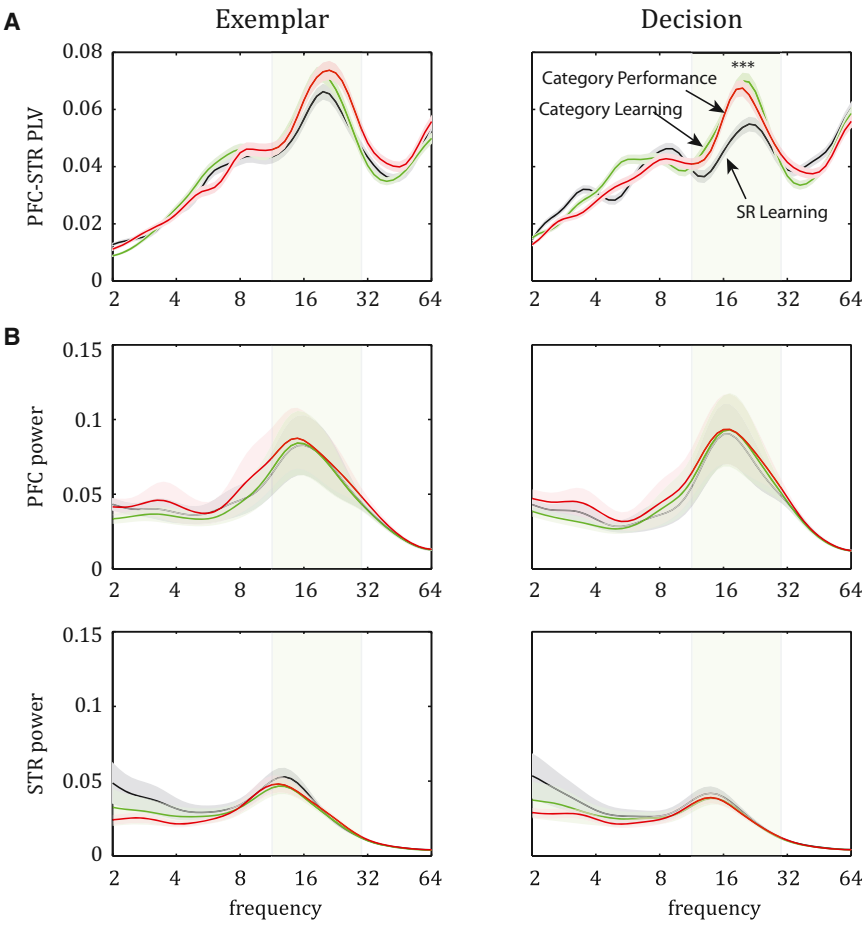

Figure 2. Frequency-Specific Oscillations in PFC and STR during Two Trial Epochs (Exemplar and Decision) Across the Three Stages of Learning

(A) Average PLV ±SEM as a function of frequency: peak synchrony between PFC and STR beta band oscillations (in this and all figures, shaded rectangle indicates the 12–30 Hz beta band) and learning-induced enhancement of this synchrony during the decision epoch (see also Figures S1 and S2; Table S1).

(B) Average spectral power (±SEM) in PFC (top) and STR (bottom) is high at the beta band, but does not change across learning stages.

learning-related changes in PLV for baseline activity (middle 500 ms time segment from the 3-s-long intertrial interval; ANOVA: $F(2,1277) = 1.04$, $p = 0.35$) (Figure S2A). The phase relationship between PFC and STR remained stable at 0° phase lag across all trial epochs and learning stages (Figure S2B).

No Changes in Oscillatory Power within the PFC or STR

The learning-related increase in PFC-STR synchrony was independent of changes in oscillatory power (i.e., the synchrony changes were not a by-product of increased oscillations per se). Note that the synchrony measure we employed (PLV) is computed only from the phase of the wave, independently from its amplitude (and thus oscillatory power). However, we also computed the frequency-dependent power of PFC and STR LFPs. To correct for the LFP's power-law decay, power was normalized to 1/frequency.

Both PFC ($n = 84$ electrodes) and STR ($n = 65$ electrodes) LFPs displayed a peak in beta (STR LFPs also displayed strong power in the 2–4 Hz delta band) (Figure 2B). Beta power was stronger in the PFC than STR, with a peak at a somewhat higher frequency (peak at 16 Hz versus 13 Hz, respectively) (Figure 2B). However, there was no change in beta oscillatory power across learning stages in either area for either the exemplar or decision epoch (Figure 2B, ANOVA in PFC: exemplar epoch $F(2,251) = 0.004$, $p = 0.99$, decision epoch $F(2,251) = 0.001$, $p = 0.99$; STR: exemplar epoch $F(2,194) = 0.49$, $p = 0.62$, decision epoch $F(2,194) = 0.18$, $p = 0.82$). This suggests that the learning-related changes in synchrony between the PFC and STR reflected changes in functional connectivity per se rather than just a general change in oscillatory dynamics. Indeed, as we will see next, learning-related changes in synchrony only occurred between the PFC and STR; there was no learning-related change in synchrony within either area.

No Changes in Synchrony within the PFC or STR

The learning-related increase in beta synchrony was limited to interactions between the PFC and STR; there was no learning-related change in beta (or any other frequency band) synchrony within either area. We performed the same analyses as above on pairs of recording sites within each area (Figures 3A and S2A). Synchrony between recording sites within the PFC ($n = 240$ electrode pairs) or STR ($n = 141$ electrode pairs) were overall greater than those between PFC and STR (within-STR average PLV was also greater than within-PFC average PLV) with a peak in the beta band (at ~20Hz). However, beta band PLV values within the PFC and STR did not change across learning stages in either the exemplar epoch (ANOVA across stages in beta-specific PLV within PFC: $F(2,719) = 0.05$, $p = 0.95$; within STR: $F(2,422) = 0.23$, $p = 0.79$) (Figure 3A, left) or the decision epoch (within PFC: $F(2,719) = 0.06$, $p = 0.94$; within STR: $F(2,422) = 0.42$, $p = 0.66$) (Figure 3A, right). Decision-epoch PLV within the PFC and within the STR was similar during SR Learning, Category Learning, and Category Performance (only 0.5%–2.12% difference across learning within PFC and 2.2%–4.4% within STR). Compare this to learning-related increases in beta band PLV of around 30% between the PFC and STR (Figure 3B, right).

Decrease in PFC-STR Synchrony during Error Trials

To determine whether the PFC-STR synchrony was related to task performance, we examined PLV from trials in which the monkeys made the incorrect behavioral choice at the end of

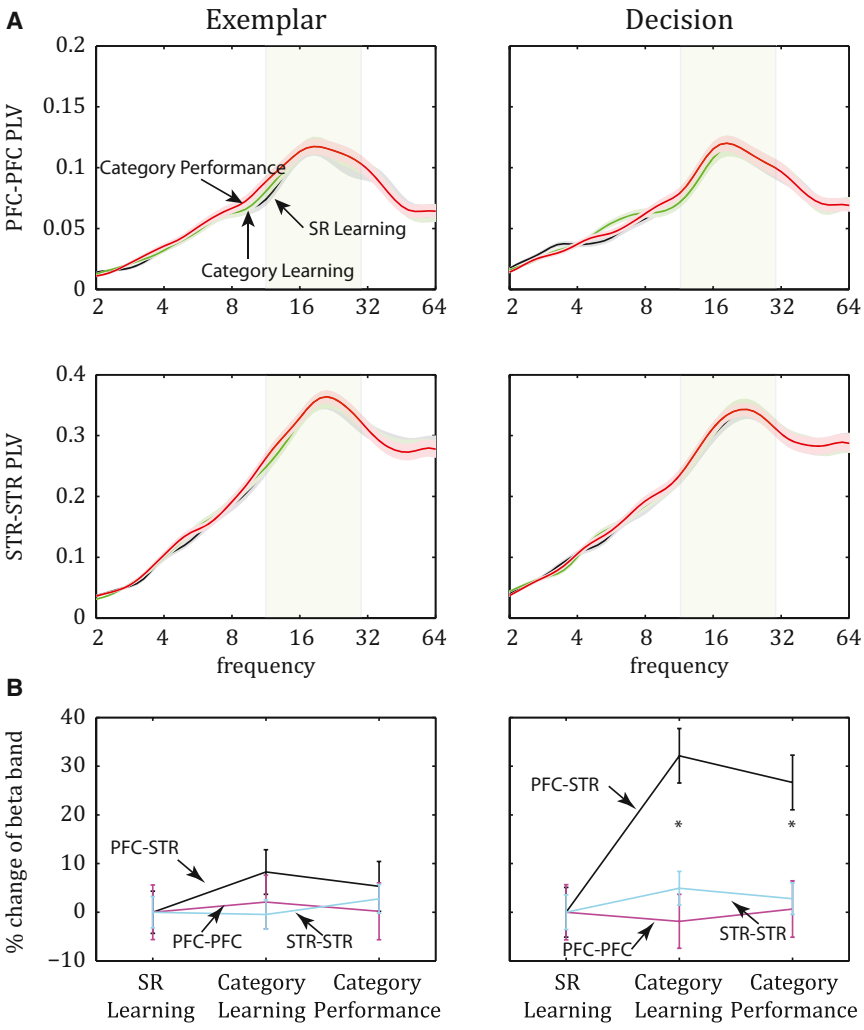

Figure 3. Synchrony between Intrinsic Pairs of Electrodes in PFC and STR

(A) Average PLV (±SEM): although intrinsic connectivity peaked at the beta band both in PFC (top) and in STR (bottom), it did not change with learning (see also Figure S2).

(B) The percent increase of synchrony between PFC and STR after the SR Learning stage during the decision epoch (right) was significantly greater than the corresponding change in synchrony of intrinsic PFC pairs (PFC-PFC) and STR pairs (STR-STR) of electrodes. Error bars indicate SEM.

the trial. This analysis was necessarily focused only on the SR Learning and Category Learning stages because the animals' asymptotic performance during Category Performance did not include sufficient error trials for their analysis.

While there was strong beta band synchrony during error trials (Figure 4A), there was no learning-related increase in beta synchrony (PLV), unlike what was seen for correct trials (see above). On the contrary, there was a significant decrease of PFC-STR beta band PLV from SR Learning to Category Learning during the exemplar epoch (Figure 4A, left; ANOVA across stages: $F(1,810) = 28.83$, $p = 10^{-7}$). Synchrony did not change significantly across the two stages in the decision epoch ($F(1,810) = 3.48$, $p = 0.06$; Figure 4A, right).

In order to compare synchrony between correct and error trials, we employed the discrimination index d′, which quantifies the difference between the mean of two sets of trials (i.e., error and correct trials), normalized to their pooled SD (Dayan and Abbott, 2001). This quantity was transformed into a z score, based on 200 random shuffles of the trials between the correct and error groups. The average z-transformed d′ indicated a significant decline in error-correct synchrony for the beta band from SR Learning to Category Learning (15–20 Hz; ANOVA on exemplar epoch d′ between SR Learning and Category Learning: $F(1,810) = 54.11$, $p = 4.7 \times 10^{-13}$; during decision epoch: $F(1,810) = 60.97$, $p = 1.8 \times 10^{-14}$). Figure 4B plots the z scores for correct trials subtracted from error trials (i.e., the average z-transformed d′). During the exemplar epoch (Figure 4B, left), note that the scores were significantly above zero in beta for SR Learning (t test for d′ relative to zero discrimination: $p = 1.7 \times 10^{-8}$), indicating greater synchrony on error trials and significantly below zero for Category Learning ($p = 2.8 \times 10^{-5}$), indicating greater beta synchrony on correct trials. For the decision epoch (Figure 4B, right), error-correct values were significantly greater than zero for SR Learning, indicating greater beta synchrony on error trials (t test, $p = 3 \times 10^{-21}$). However, during Category Learning, there was no difference in beta synchrony between correct and error trials (i.e., error-correct PLV values did not differ from zero [p = 0.81]). Therefore, we see that the shift from SR Learning to Category Learning led to changes in PFC-STR synchrony that depended on trial epoch and task performance. In the exemplar epoch, there was a significant decline of PLV during error trials (Figure 4A, left) but no change in correct trials (Figure 2A, left). In the decision epoch, there was a significant increase of PLV during correct trials (Figure 2A, right) but no change in error trials (Figure 4A, right). Note that the net effect is similar: for both exemplar and decision epochs, the transition from SR Learning to Category Learning preferentially favored the PFC-STR synchrony during correct, relative to erroneous, categorization.

Emergence of Category-Specific Patterns of Synchrony between the PFC and STR with Learning

A recent study of PFC LFPs reported rule-specific patterns of beta band synchrony between different recording sites, suggesting that beta synchrony can help form network ensembles for rules (Buschman et al., 2012). We examined whether

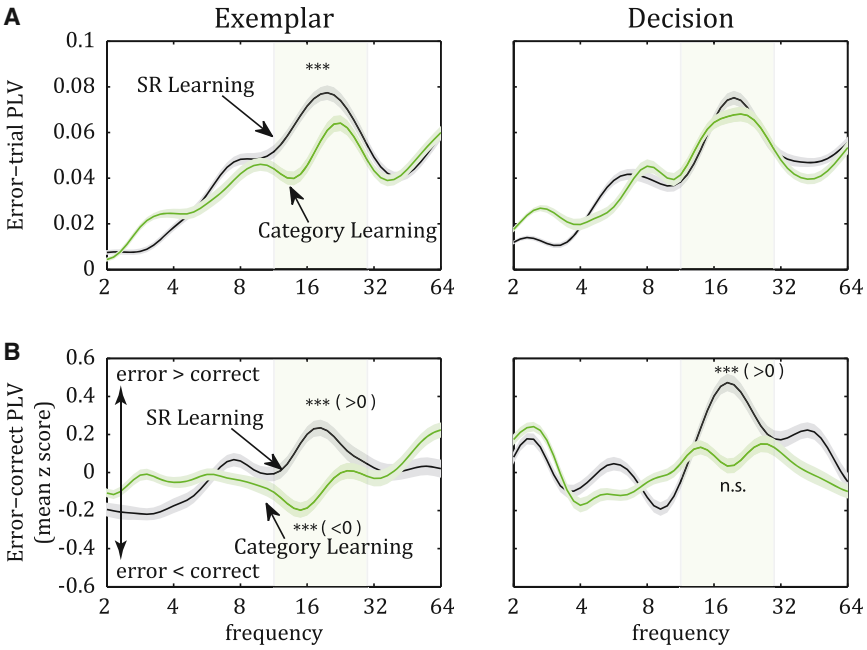

Figure 4. Analyses of PFC-STR Synchrony in Error Trials of SR Learning and Category Learning Stages

(A) Average (±SEM) PLV in error trials: in contrast to the increase of beta band synchrony observed in correct trials (Figure 2), synchrony between PFC and STR did not increase across learning stages; rather, it decreased significantly, at least during the exemplar epoch.

(B) The average (±SEM) z-transformed difference (d′) between error- and correct-trial PLV. During both trial epochs, error trials displayed stronger PFC-STR synchrony than did correct trials in the SR Learning stage, but, in the Category Learning stage, this difference was either eliminated (decision epoch) or reversed (exemplar epoch).

category-specific rhythmic networks formed in the process of category learning.

For each pair of electrodes, we computed differences in synchrony (PLV) for exemplars from the two categories using the discrimination index d′ (described above), as in our previous study of neural activity (Antzoulatos and Miller, 2011). To correct biases of the d′ metric due to variable and unequal numbers of trials, and to evaluate its statistical significance, trials were randomly shuffled 200 times between the two categories, thus generating a randomization distribution for the d′ quantity, which was then used to z transform each electrode pair's d′. In short, we used this measure to determine whether different electrode pairs showed different levels of synchrony for the two different categories (i.e., category selectivity).

Significant category-selective synchrony was observed, but only after the animals had learned the categories. During Category Performance, there was a significant increase of exemplar epoch category-selective synchrony in the beta band (peak at ~19 Hz) between the PFC and STR (Figure 5A, left) (ANOVA on category selectivity across learning stages, $F(2,1277) = 21.88$, $p = 4.5 \times 10^{-10}$; post hoc comparisons: selectivity during Category Performance greater than during SR Learning and Category Learning, $p = 5 \times 10^{-7}$). During the decision epoch, there was a significant increase of delta band category selectivity (peak at ~3 Hz, Figure 5A, right) ($F(2,1277) = 39.37$, $p = 2.6 \times 10^{-17}$; post hoc comparisons: selectivity during Category Performance greater than during SR Learning and Category Learning: $p = 10^{-11}$). Correspondingly, category-selective PFC-STR synchrony was not different from that expected by chance during the SR Learning or Category Learning stages but was significantly different from chance during Category Performance (t test for selectivity greater than zero in beta band of exemplar epoch: SR Learning, $p = 0.99$; Category Learning, $p = 0.99$; Category Performance, $p = 7.2 \times 10^{-8}$; in delta band of decision epoch: SR Learning, $p = 0.99$; Category Learning, $p = 0.99$; Category Performance, $p = 5.7 \times 10^{-16}$).

As was seen for the learning-related general increase in beta synchrony, significant category-selective synchrony was only seen between the PFC and STR. There was no significant category-selective synchrony within the PFC or STR (t test for selectivity greater than zero: SR Learning stage: exemplar epoch, within PFC $p = 0.99$, within STR $p = 0.99$, decision epoch, PFC $p = 0.14$, STR $p = 0.99$; Category Learning stage: exemplar PFC $p = 0.99$, STR $p = 0.06$, decision PFC $p = 0.99$, STR $p = 0.08$; Category Performance stage: exemplar PFC $p = 0.99$, STR $p = 0.99$, decision PFC $p = 0.27$, STR $p = 0.92$). Thus, it seems that acquisition of the categories is accompanied by development of category-specific patterns of synchrony between, but not within, the PFC and STR.

Significant category-selective beta synchrony (at ~14 Hz) during Category Performance was also seen between spikes and LFPs during the exemplar epoch, specifically between PFC multiunit spiking activity (MUA) and STR LFPs (Figure 5B; ANOVA across stages: $F(2,1239) = 19.71$, $p = 3.8 \times 10^{-9}$; post hoc comparisons: selectivity during Category Performance stage greater than during SR Learning and Category Learning stages, $p = 5 \times 10^{-6}$). This spike-LFP synchrony was significantly greater than that expected by chance during Category Performance (t test: $p = 5.3 \times 10^{-8}$) but not during SR Learning ($p = 0.49$) or Category Learning ($p = 0.90$). Importantly, spike-LFP category-selective synchrony was asymmetric. It was seen between PFC spikes and STR LFPs (above) but not between STR spikes and PFC LFPs at any of the learning stages (Figures 5B and S3A, t test: SR Learning, $p = 0.82$; Category Learning, $p = 0.96$; Category Performance, $p = 0.59$). As was seen for LFP-LFP synchrony, there was no evidence for category-specific spike-LFP synchrony within PFC or STR (Figure S3B; SR Learning stage: PFC $p = 0.96$, STR $p = 0.99$; Category Learning stage: PFC $p = 0.52$, STR $p = 0.86$; Category Performance stage: PFC $p = 0.11$, STR $p = 0.23$). Thus, it seemed that patterns of category-selective synchrony were

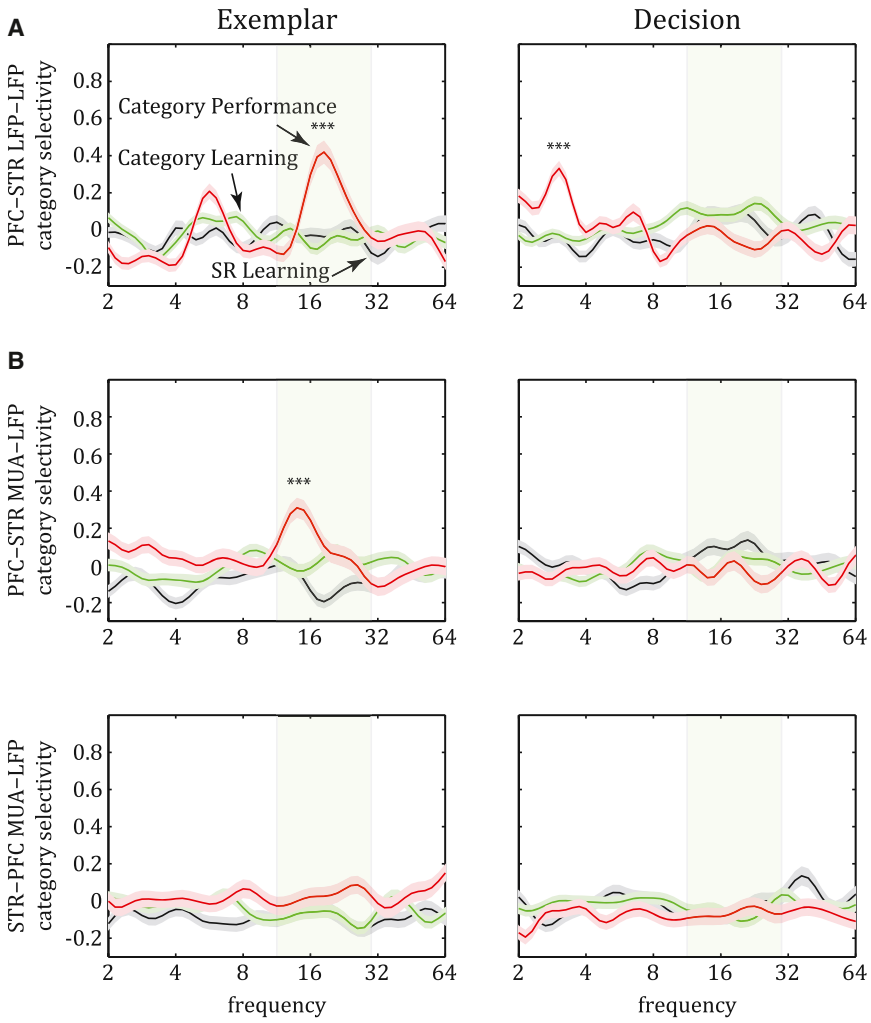

Figure 5. Category Selectivity in the Strength of PFC-STR Synchrony

(A) Synchrony between PFC and STR LFPs (average z-transformed d′ ±SEM) displayed significant category selectivity during the Category Performance stage. Category-specific synchrony was observed at the beta band during the exemplar epoch and at the delta band during the decision epoch.

(B) Similar to the LFP-LFP synchrony above, MUA-LFP synchrony (average z-transformed d′ ±SEM) between PFC-STR (spikes in PFC, LFP in STR; top) also displayed significant category selectivity at the beta band of the exemplar epoch; again, this was evident for the first time during the Category Performance stage. In contrast, the reverse direction (spikes in STR and LFP in PFC; bottom) did not show any category selectivity (see also Figure S3).

from the PFC to the STR, not the other way around and not within either area.

In our task, each category was uniquely associated with a saccade to the left or the right. Most cortical areas show activity that is biased toward processing of, and actions to, the contralateral hemifield. We therefore sought to determine whether the category-selective synchrony was primarily associated with categories signaling contralateral saccades. While LFP-LFP synchrony was seen for categories associated with both contralateral and ipsilateral saccades, there was a significant bias toward contralateral saccades for delta band category-selective synchrony during the decision epoch, when the monkeys prepared to execute the saccade (63.9% of all electrode pairs preferred contralateral saccades; $p = 0.0001$, chi-square test). By contrast, there was no contralateral or ipsilateral bias for beta band category-selective synchrony during the exemplar epoch (53.5% of all pairs preferred contralateral saccades; $p = 0.16$). Category-specific beta band spike-LFP synchrony between PFC-STR was also not biased for ipsilateral versus contralateral saccades (50.8% of all pairs preferred contralateral saccades: $p = 0.81$).

STR Exerts Larger Causal Influence on PFC than the Reverse

The measure of synchrony utilized above (PLV) is a measure of functional, not causal, connectivity, because it provides no information on the causal influence of one area on the other. Granger's test of causal connectivity can be used to indicate the degree of influence each area has on another. It evaluates how much of one area's LFP variance can be explained by the other area's LFP variance. Furthermore, this analysis can be performed at the frequency domain to identify causal influence specific to brain rhythms (Friston et al., 2013). Because Granger causality can also be affected by areas that provide common input to PFC and STR and/or intervene between the two (e.g., the rest of BG), it is also a more global measure of influence than the spike-LFP synchrony we showed above (which is more sensitive to direct neurophysiological connections between the two areas).

We analyzed the causality between PFC and STR LFPs with a nonparametric variant of the Granger causality test so the results would not hinge on the order of the multivariate autoregressive model that a parametric test would require (Dhamala et al., 2008; Roberts et al., 2013). This analysis revealed that, although both areas had causal influence on each other, STR exerted a significantly stronger causal influence on PFC than PFC on STR (i.e., STR LFPs were better predictors of PFC LFPs rather than the reverse), and this was evident across the largest part of the frequency spectrum (Figure 6A) (e.g., 20 Hz beta band at SR Learning stage, exemplar epoch: t test on magnitude of Granger causality between the two directions: $p = 10^{-45}$; decision epoch: $p = 10^{-41}$). Indeed, most of the PFC-STR electrode pairs showed a stronger influence from STR to the PFC than the other way around (exemplar epoch: 80.8% of all pairs: $p = 0.0001$, chi-square test; decision epoch: 77.2%; $p = 0.0001$). In

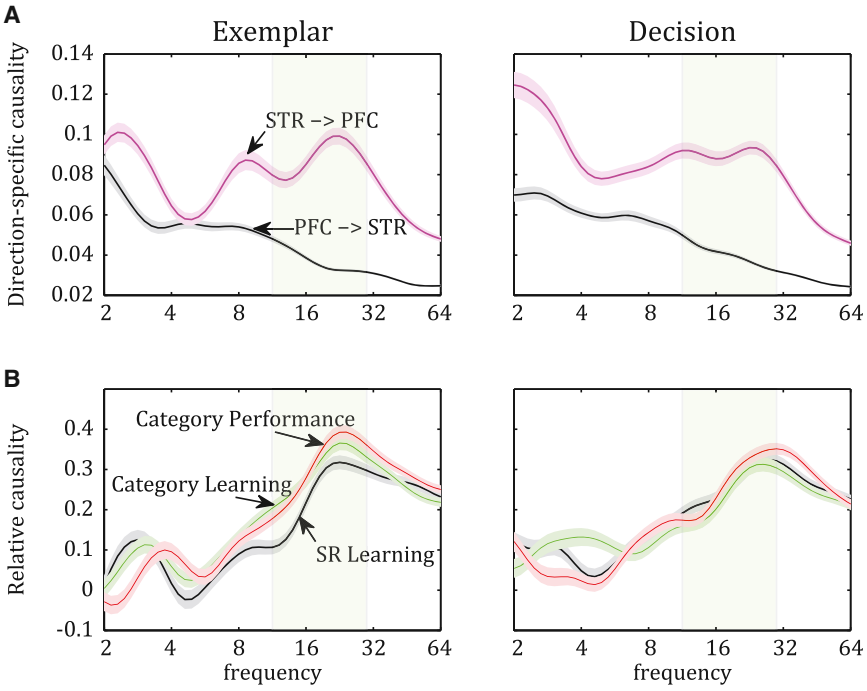

Figure 6. Analyses of Granger Causal Connectivity between PFC and STR

(A) Average Granger connectivity index ±SEM: the two directions of causal connectivity during the two trial epochs of the SR Learning stage. Striatum exerts stronger influence on the prefrontal LFPs (STR → PFC) than the other way around (PFC → STR). This difference is seen across the frequency spectrum, but especially at the beta band (shaded rectangle).

(B) Average (±SEM) relative causality (STR → PFC direction normalized to the PFC → STR direction) across learning stages. In contrast to the robust enhancement of functional connectivity at the beta band (20 Hz) with learning (Figure 2), causal connectivity did not increase significantly, suggesting that the relative influence of one area on the other did not change.

addition to their difference in magnitude of causal connectivity, the two areas also differed in the spectral profile of their causal influence on one another: PFC had the strongest influence on the low frequencies of STR LFPs (e.g., delta band), whereas STR displayed clear peak influence on both the delta and beta bands of the prefrontal LFPs (Figure 6A).

In order to evaluate learning-induced changes in the relative causal connectivity between PFC and STR, we computed a composite causality index from both directions (PFC → STR and STR → PFC) for each learning stage and trial epoch: (A−B)/(A+B), wherein A is STR → PFC causality and B is PFC → STR causality. There was little change in the direction of influence between the PFC and STR (Figure 6B) and no significant change in the 20 Hz beta band that displayed the aforementioned synchrony changes (ANOVA on causality of exemplar epoch across stages of learning: $F(2,1277) = 2.49$, $p = 0.08$; decision epoch: $F(2,1277) = 1.37$, $p = 0.25$). This suggests that the relative weight of one area's influence on the other did not change as a result of learning. Thus, while the analysis on category-selective spike-LFP synchrony (above) suggested a one-way PFC-STR synchrony, consistent with the monosynaptic connections from the PFC to STR, it appears that the polysynaptic connections from the STR back to the PFC had a greater influence on the PFC oscillations.

DISCUSSION

We found that category learning was accompanied by increased synchronization between, but not within, the PFC and striatum. Synchrony is thought to play a role in establishing functional circuitry (Engel et al., 2001; Fries, 2005; Miller and Buschman, 2013; Uhlhaas et al., 2009). Supporting this, we found that once the categories were learned, different pairs of PFC-STR recording sites showed increased synchrony for one or the other category, suggesting functional circuits for mapping category representations in the PFC to the appropriate motor program in the BG. Spike-LFP synchrony did suggest that the category-specific synchrony was, in fact, asymmetric between the PFC and STR, reflecting the asymmetric monosynaptic projections between them. However, causal connectivity analysis suggested that the polysynaptic projections from the STR back to the PFC exerted a greater influence. This is consistent with models positing that the STR (through the BG) continually "trains" the PFC (Antzoulatos and Miller, 2011; Ashby et al., 2007; Djurfeldt et al., 2001; Houk and Wise, 1995; Miller and Buschman, 2008; Pasupathy and Miller, 2005; Seger and Miller, 2010).

The learning-related increases in PFC-STR synchrony seemed functional. First, they were not simply due to an overall increase in oscillatory power. Second, they were only seen during the trial and not in baseline activity. Third, they were specific to synchrony between the areas; there were no synchrony changes within PFC or STR. Finally, error trials (incorrect choices) did not display the same increase in beta synchrony that correct trials did. Curiously, error trials during SR Learning displayed stronger PFC-STR beta synchrony than did correct trials. This reversed once the animals advanced to Category Learning. SR learning is well known to rely on the BG (Packard and Knowlton, 2002), and striatal neurons display rapid acquisition of SR associations (Antzoulatos and Miller, 2011; Pasupathy and Miller, 2005). It is possible that stronger error trial beta synchrony between the STR and PFC interfered with the ability of STR to map the stimulus to the correct motor response during SR Learning. Indeed, excessive synchrony of cortex-BG networks is seen during Parkinsonian motor symptoms (Hammond et al., 2007; Marreiros et al., 2012).

Learning-related effects in the beta band are consistent with prior observations that beta band (12–30 Hz) oscillations are prominent in frontal cortex (Puig and Miller, 2012; Siegel et al., 2009) while gamma band oscillations predominate in posterior

cortex (Fries, 2009), that cortical beta versus gamma are associated with top-down (feedback) versus bottom-up (feedforward) processing (Buschman and Miller, 2007; Engel and Fries, 2010), and beta band oscillations synchronize striatal neurons in monkeys performing oculomotor tasks (Courtemanche et al., 2003). It should be noted that "beta band" may include more than one type of oscillation with distinct neurophysiological mechanisms and functions (Cannon et al., 2013). Indeed, the different results from this study showed peaks at different frequencies within the beta band. A dissection of the contributions of different beta sub-bands was beyond the scope of our study.

The learning-related changes in PFC-STR synchrony parallel the changes in category learning-related changes in single-neuron activity previously seen in this data set (Antzoulatos and Miller, 2011). During SR Learning, STR spiking activity was an earlier predictor of the corresponding saccade than the PFC. However, when monkeys advanced to Category Learning, PFC neurons began predicting the saccade associated with each category before the STR. One result of this was that PFC and STR neurons showed more overlap of their task-related spiking activity during and after Category Learning, relative to SR Learning. This overlap was in the decision epoch, just before the behavioral response. This is when we also first observed the learning-related increase in PFC-STR beta synchrony.

Category-selective beta synchrony could serve to communicate the categorical decision from the PFC to the STR. It occurred well before the motor response, during exemplar presentation, and did not show a contralateral motor bias. By contrast, category-specific delta synchrony occurred when the monkeys were about to make their motor response, and it was contralaterally biased. This could reflect recruitment of PFC and striatum in a larger network for motor acts. Low frequency oscillations (like delta and theta) have been associated with long-range synchronization among spatially diverse systems in the context of decision making, attention, and memory (Haegens et al., 2011; Schroeder and Lakatos, 2009; Watrous et al., 2013). Delta band synchronization (at least in visual cortex) is also observed during eye movements (Bosman et al., 2009; Ito et al., 2013). It should be noted that an emergence of category selectivity in the absence of a change in general synchrony suggests that synchrony during the preferred category increases, while synchrony during the nonpreferred category decreases, thus offsetting each other when synchrony across all trials is computed.

Dopamine may play a role in learning-related changes in synchrony. It mediates plasticity of excitatory corticostriatal connections. Because the phasic dopamine release that signals reward-prediction errors induces long-term potentiation of active cortical synapses onto medium spiny striatal neurons of the direct pathway (Gerfen and Surmeier, 2011; Lerner and Kreitzer, 2011)—i.e., the pathway that closes the PFC-BG-thalamus-PFC loop—it may also be responsible for increasing the synchronization between PFC and STR. Although dopamine is also known to affect the activity of prefrontal neurons during SR learning (Puig and Miller, 2012) and working memory (Arnsten et al., 2012), it is thought to be of less consequence for corticocortical than for corticostriatal synapses (Ashby et al., 2007; Miller and Buschman, 2008). This may be why we found that corticostriatal synchrony was enhanced while corticocortical synchrony was not. It is also possible that corticocortical (and striatostriatal) connections require more experience for functional circuitry to be established. Rule-specific beta synchronization within the PFC has been observed (Buschman et al., 2012), but it was for highly familiar rules and not during new learning, as in this study.

The lack of learning-related changes in synchrony within the PFC and STR was in contrast to changes between them. Although we cannot exclude a ceiling effect for intrinsic synchrony, it is unlikely. The PFC-PFC synchrony was weaker than STR-STR synchrony, and yet it did not change with learning. Interestingly, the lateral connections between the STR medium spiny neurons are sparse, with high failure rate (Plenz, 2003). The stronger intrinsic STR synchrony, therefore, may arise from a common signal external to the STR, such as the substantia nigra pars compacta (SNpc): its dopaminergic neurons fire spikes at highly regular intervals and could have pacemaking functions (Surmeier et al., 2005). Recent studies have also suggested that striatal synchrony can be regulated by the subthalamic nucleus (Marreiros et al., 2012).

We found that the STR had a stronger net influence on the PFC than PFC on STR. This causal influence may be task dependent. In a stimulus-stimulus association task, the PFC was reported to exert larger causal influence on STR, consistent with their monosynaptic connections (Ma et al., 2013). However, the BG is indeed thought to exert a strong influence on frontal cortex (Ashby et al., 2007; Seger, 2008). The globus pallidus (which receives direct projections from the STR) affects the timing and presumably strength of thalamocortical communication (Goldberg et al., 2013) and also sends monosynaptic feedback signals to STR (Gerfen and Surmeier, 2011; Lerner and Kreitzer, 2011). The dopaminergic projection from SNpc is denser (i.e., presumably stronger) to STR than to the PFC (Lynd-Balta and Haber, 1994). Any of these signals, therefore, could shape both the PFC but mostly the STR rhythms, thus making the STR LFPs better predictors of PFC signals. The greater causal influence of the STR on the PFC is consistent with the hypothesis that STR learns about individual exemplars and then, via the rest of the BG, "trains" their categories in the PFC (Antzoulatos and Miller, 2011; Pasupathy and Miller, 2005; Seger and Miller, 2010). However, this process is continual and recursive: once the categories are learned, they can be fed into the STR for further learning, which may explain why, after learning, we found category-specific synchrony from the PFC to the STR.

EXPERIMENTAL PROCEDURES

Animals

Data were acquired from two adult female macaque monkeys, maintained in accordance with the National Institutes of Health guidelines and the policies of the Massachusetts Institute of Technology Committee for Animal Care.

Task

The details of the task have been presented previously (Antzoulatos and Miller, 2011). Briefly, the animals initiated a trial by fixating on a central target. While the animals maintained fixation, a randomly chosen category exemplar from either category was presented for 0.6 s. Trials from both categories were randomly interleaved throughout the session. One second after the exemplar

display offset, two saccade targets appeared on the left and right of the center of fixation, and the animal had to make a single, direct saccade to the correct target for reward. Category exemplars were random 7-dot constellations, generated through distortion of the corresponding prototype (Figure 1).

Neurophysiology

Simultaneous recordings from PFC and STR were performed using multielectrode arrays, lowered at different PFC and STR sites every day. LFPs were decomposed to their individual frequency components using wavelet analysis. Functional connectivity (i.e., frequency-specific synchrony) between pairs of LFP signals was computed as a PLV over two 500 ms trial epochs: the exemplar epoch (last 500 ms of exemplar display) and the decision epoch (last 500 ms before the animals' saccade). PLV computes the circular mean of a sample of phase differences (phase lags) and varies between 0 (when all phase lags are uniformly distributed across 360 degrees) and 1 (when all phase lags are concentrated at a single phase). Similar results on synchrony were obtained when we computed coherence or pairwise phase consistency. For differences in synchrony between two sets of trials (e.g., correct versus error, or category A versus B), we used the same selectivity metric (discrimination index d′) we employed previously (Antzoulatos and Miller, 2011). To correct for sampling bias, we randomly shuffled the trials between the two sets 200 times, thus generating a randomization distribution that was used as surrogate data. The observed d′ values were subsequently transformed into z scores based on the surrogate data set and averaged across the population of electrode pairs. Finally, causal connectivity analyses relied on a nonparametric Granger test, which evaluates the degree to which signal A can predict (i.e., explain the variance of) the frequency-specific oscillations of signal B. All computations were done using MATLAB (see Supplemental Information for more details).

SUPPLEMENTAL INFORMATION

Supplemental Information includes three figures, one table, and Supplemental Experimental Procedures and can be found with this article online at http://dx.doi.org/10.1016/j.neuron.2014.05.005.

ACKNOWLEDGMENTS

The authors thank B. Gray, S. Koopman, and D. Ouellette for technical assistance; S. Brincat, J. Donoghue, S. Kornblith, R. Loonis, M. Lundqvist, M. Moazami, V. Puig, J. Rose, J. Roy, and M. Silver for helpful discussions; and M. Wicherski for comments on the manuscript. This work was funded by the National Institute of Mental Health (5R01MH065252-12) and the Picower Foundation.

Accepted: May 1, 2014
Published: June 12, 2014

REFERENCES

Antzoulatos, E.G., and Miller, E.K. (2011). Differences between neural activity in prefrontal cortex and striatum during learning of novel abstract categories. Neuron *71*, 243–249.

Arnsten, A.F., Wang, M.J., and Paspalas, C.D. (2012). Neuromodulation of thought: flexibilities and vulnerabilities in prefrontal cortical network synapses. Neuron *76*, 223–239.

Ashby, F.G., Ennis, J.M., and Spiering, B.J. (2007). A neurobiological theory of automaticity in perceptual categorization. Psychol. Rev. *114*, 632–656.

Bosman, C.A., Womelsdorf, T., Desimone, R., and Fries, P. (2009). A microsaccadic rhythm modulates gamma-band synchronization and behavior. J. Neurosci. *29*, 9471–9480.

Brovelli, A., Ding, M., Ledberg, A., Chen, Y., Nakamura, R., and Bressler, S.L. (2004). Beta oscillations in a large-scale sensorimotor cortical network: directional influences revealed by Granger causality. Proc. Natl. Acad. Sci. USA *101*, 9849–9854.

Buschman, T.J., and Miller, E.K. (2007). Top-down versus bottom-up control of attention in the prefrontal and posterior parietal cortices. Science *315*, 1860–1862.

Buschman, T.J., Denovellis, E.L., Diogo, C., Bullock, D., and Miller, E.K. (2012). Synchronous oscillatory neural ensembles for rules in the prefrontal cortex. Neuron *76*, 838–846.

Cannon, J., McCarthy, M.M., Lee, S., Lee, J., Borgers, C., Whittington, M.A., and Kopell, N. (2013). Neurosystems: brain rhythms and cognitive processing. Eur. J. Neurosci. *39*, 705–719.

Courtemanche, R., Fujii, N., and Graybiel, A.M. (2003). Synchronous, focally modulated beta-band oscillations characterize local field potential activity in the striatum of awake behaving monkeys. J. Neurosci. *23*, 11741–11752.

Daitch, A.L., Sharma, M., Roland, J.L., Astafiev, S.V., Bundy, D.T., Gaona, C.M., Snyder, A.Z., Shulman, G.L., Leuthardt, E.C., and Corbetta, M. (2013). Frequency-specific mechanism links human brain networks for spatial attention. Proc. Natl. Acad. Sci. USA *110*, 19585–19590.

Daw, N.D., Niv, Y., and Dayan, P. (2005). Uncertainty-based competition between prefrontal and dorsolateral striatal systems for behavioral control. Nat. Neurosci. *8*, 1704–1711.

Dayan, P., and Abbott, L.F. (2001). Theoretical Neuroscience. (Cambridge: The MIT Press).

Dhamala, M., Rangarajan, G., and Ding, M. (2008). Analyzing information flow in brain networks with nonparametric Granger causality. Neuroimage *41*, 354–362.

Djurfeldt, M., Ekeberg, O., and Graybiel, A.M. (2001). Cortex-Basal Ganglia Interaction and Attractor States. Neurocomputing *38-40*, 573–579.

Engel, A.K., and Fries, P. (2010). Beta-band oscillations—signalling the status quo? Curr. Opin. Neurobiol. *20*, 156–165.

Engel, A.K., Fries, P., and Singer, W. (2001). Dynamic predictions: oscillations and synchrony in top-down processing. Nat. Rev. Neurosci. *2*, 704–716.

Fries, P. (2005). A mechanism for cognitive dynamics: neuronal communication through neuronal coherence. Trends Cogn. Sci. *9*, 474–480.

Fries, P. (2009). Neuronal gamma-band synchronization as a fundamental process in cortical computation. Annu. Rev. Neurosci. *32*, 209–224.

Friston, K., Moran, R., and Seth, A.K. (2013). Analysing connectivity with Granger causality and dynamic causal modelling. Curr. Opin. Neurobiol. *23*, 172–178.

Gerfen, C.R., and Surmeier, D.J. (2011). Modulation of striatal projection systems by dopamine. Annu. Rev. Neurosci. *34*, 441–466.

Goldberg, J.H., Farries, M.A., and Fee, M.S. (2013). Basal ganglia output to the thalamus: still a paradox. Trends Neurosci. *36*, 695–705.

Haegens, S., Nácher, V., Hernández, A., Luna, R., Jensen, O., and Romo, R. (2011). Beta oscillations in the monkey sensorimotor network reflect somatosensory decision making. Proc. Natl. Acad. Sci. USA *108*, 10708–10713.

Hammond, C., Bergman, H., and Brown, P. (2007). Pathological synchronization in Parkinson's disease: networks, models and treatments. Trends Neurosci. *30*, 357–364.

Hipp, J.F., Engel, A.K., and Siegel, M. (2011). Oscillatory synchronization in large-scale cortical networks predicts perception. Neuron *69*, 387–396.

Houk, J.C., and Wise, S.P. (1995). Distributed modular architectures linking basal ganglia, cerebellum, and cerebral cortex: their role in planning and controlling action. Cereb. Cortex *5*, 95–110.

Ito, J., Maldonado, P., and Grün, S. (2013). Cross-frequency interaction of the eye-movement related LFP signals in V1 of freely viewing monkeys. Front Syst Neurosci *7*, 1.

Lachaux, J.P., Rodriguez, E., Martinerie, J., and Varela, F.J. (1999). Measuring phase synchrony in brain signals. Hum. Brain Mapp. *8*, 194–208.

Lerner, T.N., and Kreitzer, A.C. (2011). Neuromodulatory control of striatal plasticity and behavior. Curr. Opin. Neurobiol. *21*, 322–327.

Lynd-Balta, E., and Haber, S.N. (1994). The organization of midbrain projections to the ventral striatum in the primate. Neuroscience *59*, 609–623.

Ma, C., Pan, X., Wang, R., and Sakagami, M. (2013). Estimating causal interaction between prefrontal cortex and striatum by transfer entropy. Cogn Neurodyn *7*, 253–261.

Marreiros, A.C., Cagnan, H., Moran, R.J., Friston, K.J., and Brown, P. (2012). Basal ganglia-cortical interactions in Parkinsonian patients. Neuroimage *66C*, 301–310.

Miller, E.K., and Buschman, T.J. (2008). Rules through recursion: How interactions between the frontal cortex and basal ganglia may build abstract, complex rules from concrete, simple ones. In Neuroscience of Rule-Guided Behavior, S.A. Bunge and J.D. Wallis, eds. (New York: Oxford University Press).

Miller, E.K., and Buschman, T.J. (2013). Cortical circuits for the control of attention. Curr. Opin. Neurobiol. *23*, 216–222.

Packard, M.G., and Knowlton, B.J. (2002). Learning and memory functions of the Basal Ganglia. Annu. Rev. Neurosci. *25*, 563–593.

Padmanabhan, A., Lynn, A., Foran, W., Luna, B., and O'Hearn, K. (2013). Age related changes in striatal resting state functional connectivity in autism. Front Hum Neurosci *7*, 814.

Pasupathy, A., and Miller, E.K. (2005). Different time courses of learning-related activity in the prefrontal cortex and striatum. Nature *433*, 873–876.

Plenz, D. (2003). When inhibition goes incognito: feedback interaction between spiny projection neurons in striatal function. Trends Neurosci. *26*, 436–443.

Puig, M.V., and Miller, E.K. (2012). The role of prefrontal dopamine D1 receptors in the neural mechanisms of associative learning. Neuron *74*, 874–886.

Reber, P.J., Stark, C.E., and Squire, L.R. (1998). Cortical areas supporting category learning identified using functional MRI. Proc. Natl. Acad. Sci. USA *95*, 747–750.

Roberts, M.J., Lowet, E., Brunet, N.M., Ter Wal, M., Tiesinga, P., Fries, P., and De Weerd, P. (2013). Robust gamma coherence between macaque V1 and V2 by dynamic frequency matching. Neuron *78*, 523–536.

Schroeder, C.E., and Lakatos, P. (2009). Low-frequency neuronal oscillations as instruments of sensory selection. Trends Neurosci. *32*, 9–18.

Seger, C.A. (2008). How do the basal ganglia contribute to categorization? Their roles in generalization, response selection, and learning via feedback. Neurosci. Biobehav. Rev. *32*, 265–278.

Seger, C.A., and Miller, E.K. (2010). Category learning in the brain. Annu. Rev. Neurosci. *33*, 203–219.

Seger, C.A., Poldrack, R.A., Prabhakaran, V., Zhao, M., Glover, G.H., and Gabrieli, J.D. (2000). Hemispheric asymmetries and individual differences in visual concept learning as measured by functional MRI. Neuropsychologia *38*, 1316–1324.

Siegel, M., Warden, M.R., and Miller, E.K. (2009). Phase-dependent neuronal coding of objects in short-term memory. Proc. Natl. Acad. Sci. USA *106*, 21341–21346.

Surmeier, D.J., Mercer, J.N., and Chan, C.S. (2005). Autonomous pacemakers in the basal ganglia: who needs excitatory synapses anyway? Curr. Opin. Neurobiol. *15*, 312–318.

Torrence, C., and Compo, G.P. (1998). A Practical Guide to Wavelet Analysis. Bull. Am. Meteorol. Soc. *79*, 61–78.

Uhlhaas, P.J., and Singer, W. (2012). Neuronal dynamics and neuropsychiatric disorders: toward a translational paradigm for dysfunctional large-scale networks. Neuron *75*, 963–980.

Uhlhaas, P.J., Pipa, G., Lima, B., Melloni, L., Neuenschwander, S., Nikolić, D., and Singer, W. (2009). Neural synchrony in cortical networks: history, concept and current status. Front Integr Neurosci *3*, 17.

Vogels, R., Sary, G., Dupont, P., and Orban, G.A. (2002). Human brain regions involved in visual categorization. Neuroimage *16*, 401–414.

Watrous, A.J., Tandon, N., Conner, C.R., Pieters, T., and Ekstrom, A.D. (2013). Frequency-specific network connectivity increases underlie accurate spatiotemporal memory retrieval. Nat. Neurosci. *16*, 349–356.

Yoon, J.H., Minzenberg, M.J., Raouf, S., D'Esposito, M., and Carter, C.S. (2013). Impaired prefrontal-basal ganglia functional connectivity and substantia nigra hyperactivity in schizophrenia. Biol. Psychiatry *74*, 122–129.

Neuron, Volume *83*

Supplemental Information

Increases in Functional Connectivity between Prefrontal Cortex and Striatum during Category Learning

Evan G. Antzoulatos and Earl K. Miller

Inventory of Supplemental Information

Figure S1

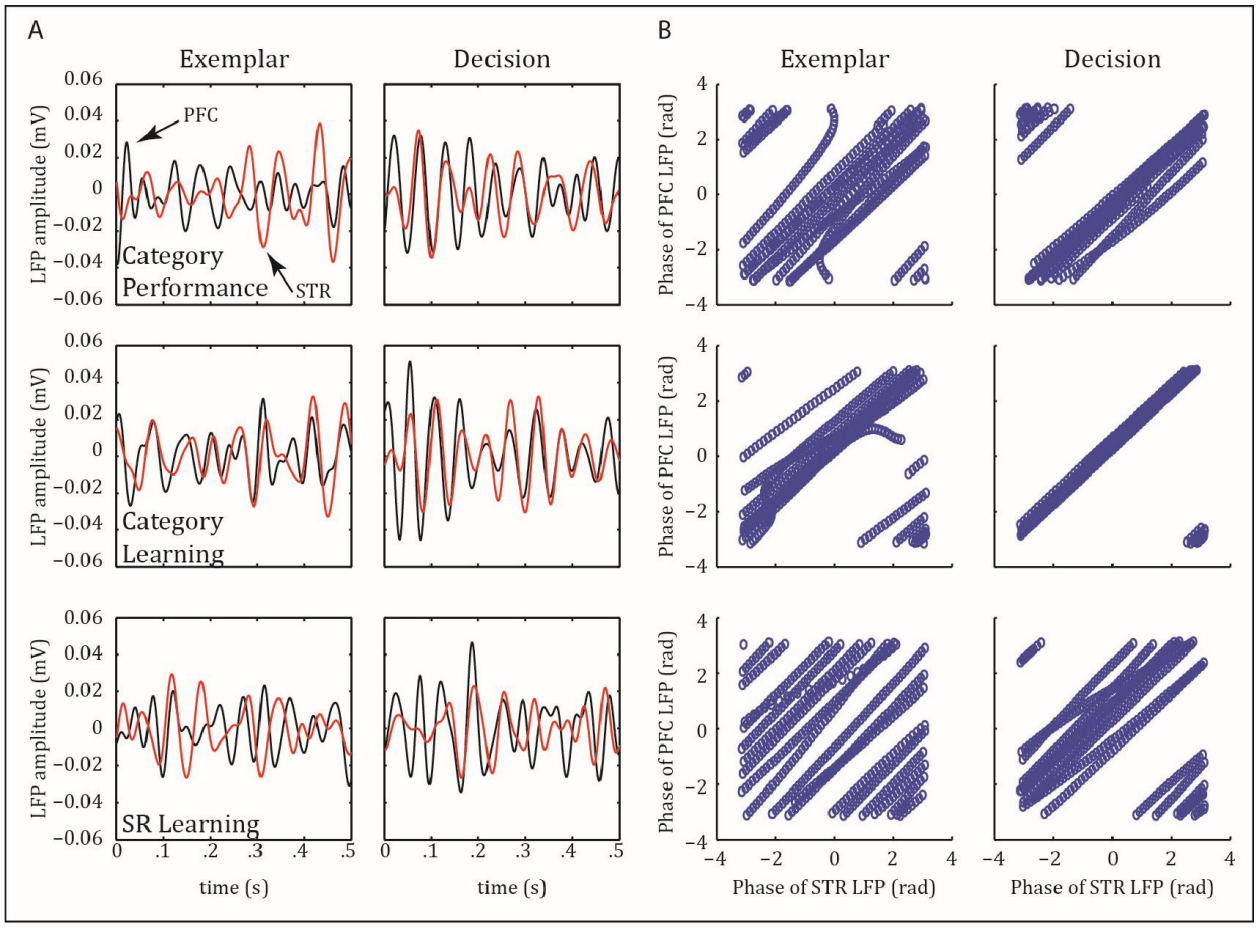

Figure S1 – Single-trial examples of synchrony: A. Single-trial simultaneous LFP recordings from a PFC electrode (black line) and a STR electrode (red line), as a function of time (x axis), trial epoch (left column: exemplar, right column: decision), and experimental stage (bottom row: SR Learning, middle row: Category Learning, top row: Category Performance). The LFP signals have been passband-filtered to illustrate the beta frequency band (12-30 Hz). Synchronization of the 2 LFP signals increases during the decision epoch of the Category Learning and Category Performance stages compared to the SR Learning stage. **B.** Scatterplots of instantaneous 20-Hz phase of the same LFP signals as in A. The appearance of continuous oblique lines is generated by virtue of the LFP's autoregressive nature, whereby all phases from -3.14 to +3.14 radians are consecutively recorded. Increased synchrony in the decision epoch of the Category Learning and Category Performance stages is obvious as a decrease in the spread of the PFC and STR phases, compared to the other epochs and learning stages.

Figure S2

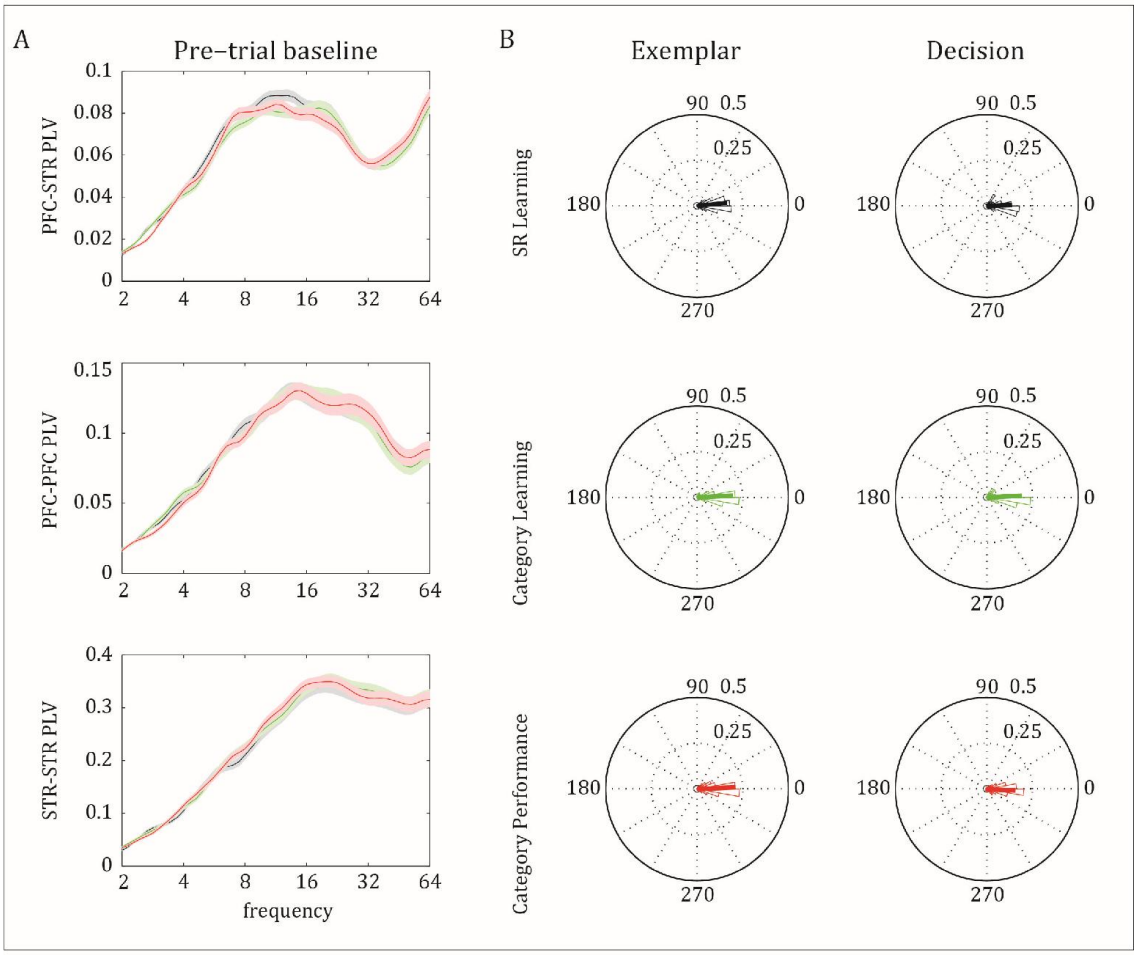

Figure S2 - Synchrony between prefrontal cortex and striatum: A. Average PLV (±SEM) across all electrode pairs between prefrontal cortex (PFC) and striatum (STR; top), within PFC (middle), and within STR (bottom) across the 3 stages of learning (same color coding as in Figs 2 and 3) during the pre-trial baseline (500 ms at the middle of the 3-s ITI). No changes in synchrony are observed, contrary to the PFC-STR synchrony of the decision epoch (Fig. 2), which increased significantly from SR Learning to Category Learning. **B.** Circular probability distribution of phase-lags (in degrees) between the PFC and STR LFPs during the exemplar and decision epochs of the 3 learning stages. Thick lines indicate average phase-lag.

Figure S3

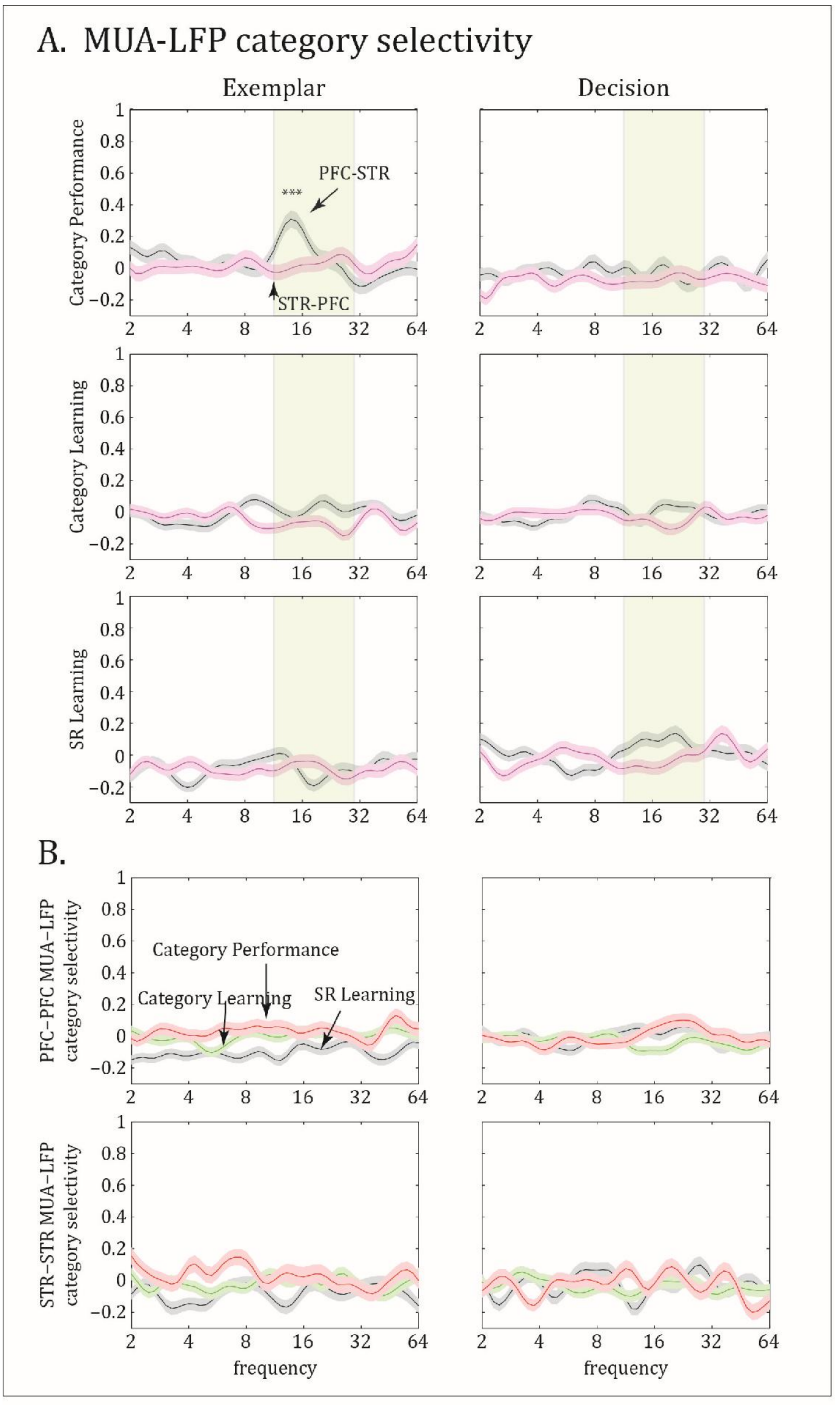

Figure S3 - Category-selective spike-LFP synchrony: A. Comparison between the 2 directions of spike-LFP synchrony: spikes in PFC and LFP in STR (PFC-STR) vs. spikes in STR and LFP in PFC (STR-PFC). Average (±SEM) category-selective synchrony (z-transformed d'), during the exemplar and decision epochs of the 3 learning stages. **B.** Average (±SEM) category-selective spike-LFP synchrony (z-transformed d') within PFC (top) and within STR (bottom), across the 3 learning stages during the exemplar and decision epochs.

Table S1

		Exemplar		Decision	
		mean	SEM	mean	SEM
Observed data PLV	Category Performance	0.4663	0.0038	0.4634	0.0033
	Category Learning	0.4656	0.0033	0.4697	0.0033
	SR Learning	0.4571	0.0031	0.4506	0.0029
Surrogate data PLV	Category Performance	0.3925	0.0007	0.3937	0.0007
	Category Learning	0.3913	0.0005	0.3977	0.0006
	SR Learning	0.3885	0.0005	0.3964	0.0007

Table S1 – Synchrony in observed and surrogate data. Mean PLV and the corresponding SEM of all PFC-STR pairs of electrodes as a function of trial epoch and experimental stage, in observed, uncorrected data (top 3 rows) and in surrogate data (bottom 3 rows). Surrogate data were generated by randomly shuffling the trials 200 times prior to computation of PLV. The surrogate-data PLV was an estimate of the bias in the PLV measure, and, to generate the main paper's results, the surrogate-data PLV was subtracted from the observed PLV. This correction was implemented at each trial.

Supplemental Experimental Procedures

Animals

Data were collected from 2 adult female rhesus monkeys (*Macaca mulatta*), 5-9 kg. The animals were taken care of in accordance with the National Institutes of Health guidelines and the policies of the Massachusetts Institute of Technology Committee for Animal Care. We had spent approx. 1.5 years training the animals on this task and exploring various different experimental designs before we started collecting neurophysiological data using the current design (see below). Both animals were trained on the category learning task until they reached similar levels of proficiency.

Task Design

The task design is shown in Fig. 1 and has been described in detail in our previous report from this dataset (Antzoulatos and Miller, 2011). Experimental control was implemented via Cortex (NIMH, Laboratory of Neuropsychology), infrared eye-tracking via Eyelink 1000 (SR Research Ltd, Mississauga, Canada) and neurophysiological recordings via the MAP system (Plexon Inc, Dallas TX). Visual stimuli were presented at full contrast, on a CRT monitor (at a distance of approx. 50 cm from the animal), refreshing at 100 Hz. Trials began when the animal maintained fixation on a central target for 0.7 s, following which, a randomly chosen exemplar from either category was presented for 0.6 s. One second after the offset of the exemplar, the fixation target was extinguished and 2 saccade targets appeared at 5^{o} to the left and right of the center of fixation. The animal had to make a single and direct saccade to the correct target within 1s, and maintain fixation on it for 200 ms for reward (drops of juice). In the case of incorrect response (error trials), there was a 5-s timeout, during which the exemplar was presented again, at the location of the correct target.

Category exemplars were static constellations of 7 randomly located dots (0.4^{o} in diameter; Fig. 1), and subtended a 6x6-degree spatial window, centered on the fixation target. For each daily recording session, we started by constructing a new pair of category prototypes. We took certain precautions (Antzoulatos and Miller, 2011; Vogels et al., 2002) to ensure an intermediate level of task difficulty and to increase the likelihood that the animals would learn the new categories in a single, daily, recording session (no categories were tested in more than 1 sessions): Within each prototype, all dots had to be more than 0.8^{o} away from each other (i.e., a distance equal to 2 dots), no more than 3 pairs of dots between prototypes were allowed to be closer than 1^{o}, and the average Euclidean distance between prototypes had to be between 1.6^{o} - 2.2^{o}. The next step was to create the category exemplars. To do so, each dot of the corresponding prototype was shifted to a random direction and distance from its original location. Distance from original location was tiered at 5 levels, each tier being one extra dot-diameter (0.4^{o}) away from the original location. The probability of each dot to land in any one of the 5 tiers was determined based on the originally published levels of distortion 2 and 3 (Antzoulatos and Miller, 2011; Posner et al., 1967). This led the majority of dots (63%) to shift by only 1 dot away (i.e. to tier 1). However, because the direction of shift could vary randomly by 360^{o} and independently for each of the 7 dots comprising the exemplar, the overall difference of an exemplar from the original prototype was substantial. No dot was allowed to stay in the same location as in the prototype, or at a distance closer than 0.8^{o} from another dot, and no more than 2 pairs of dots across exemplars could be closer than 0.5^{o} (approx. 1 dot-diameter).

On each trial, a randomly chosen exemplar was tested, with trials from both categories randomly interleaved throughout the recording session. The animals advanced through a minimum of 8 blocks, each of which included twice as many exemplars as the block before it (block 1 included 1 exemplar per category). Each block was complete when the animals' performance reached 80% correct at the last 20 trials (all analyses were performed on the minimum of 16 correct trials per block). No exemplar was allowed to be tested in more than 2 consecutive blocks. The behavioral performance criterion we employed led some blocks to be terminated before all exemplars had been tested. It was necessary to avoid prolonging a block too much, so the animal would not form habitual SR associations that would impede abstraction of the essence of each category (Antzoulatos and Miller, 2011). Distinction of learning in 3 stages relied on the same criteria we previously employed (Antzoulatos and Miller, 2011): The first 2 blocks in each experiment were assigned to learning stage 1 (SR Learning) because they only tested 1-2 exemplars per category, whose frequent repetitions allowed for learning of individual SR associations. All blocks after the 2nd, and until a category performance criterion was met (see below), were classified as learning stage 2 (Category Learning). At this stage, the likelihood of any single exemplar to be repeated was gradually diminishing, as more and more exemplars were introduced in each block. We considered category learning to be complete when the animals could classify correctly the majority (75%) of each category's exemplars on their first trial. The first 2 blocks meeting this criterion were classified as stage 3 (Category Performance), and asymptotic performance at this stage relied almost exclusively on a single trial per exemplar. The neurophysiological results were averaged across all blocks of each stage.

Neural Recordings and Data Analysis

Guided by the animals' structural MRI images, simultaneous multi-electrode recordings were made from the right lateral prefrontal cortex (PFC; dorsal and ventral regions) and the head and body of the right caudate nucleus of the striatum (STR; see Antzoulatos and Miller, 2011 for precise anatomical locations). Two custom-made multi-electrode arrays (8-16 tungsten electrodes, FHC) were lowered at different sites in the animals' brain every day of recording. Because the electrodes could be guided either individually or in pairs, apart from varying their anteroposterior and mediolateral coordinates, we could also vary their exact depth so as to maximize the yield of neural signals. Electrode recordings were first fed to a unity-gain headstage and were referenced to ground. Local field potentials (LFPs) were separated from spiking signals online at the preamplifier, using a 0.7Hz - 300Hz bandpass filter, were amplified x1000, and then sampled at 1 KHz rate. To ensure that only signals from active regions of the brain were collected, LFPs were recorded only from sites that also displayed spiking activity (a total of 84 PFC sites and 65 STR sites). Line frequency noise (60 Hz) was removed from the signal offline, by applying a 10th-order Butterworth bandstop filter (59Hz - 61Hz) at both forward and backward time directions. To remove any stimulus-evoked potentials added on top of the ongoing oscillations, prior to wavelet transform, all time-aligned LFP signals were mean centered, that is, the cross-trial average time-locked LFP signal (separate by category and outcome) was subtracted from each trial's LFP. All data analyses were performed on MATLAB (Mathworks, Natick MA), and statistical tests were corrected for multiple comparisons.

Spectral decomposition of LFPs relied on a wavelet transform by convolution of the LFP signal with a Morlet wavelet (Torrence and Compo, 1998), at 5 octaves from 2-64 Hz, at a frequency resolution of 0.1 octave. Wavelet analyses were conducted based on the MATLAB-based software Wavelet, offered by C. Torrence and G. Compo at the URL: http://atoc.colorado.edu/research/wavelets/.

After wavelet transform, the frequency-specific phase of each wave (inverse tangent of real and imaginary components) was extracted using the MATLAB function *angle* and the amplitude (from Pythagorean equation with the real and imaginary components as x and y) using the function *abs*. Spectral power was computed as the squared amplitude, and normalized to frequency^{-1} to correct for the power-law decay and enhance visibility of the higher frequencies (Siegel et al., 2009). Synchrony between pairs of LFP signals was evaluated as a Phase-Locking Value (PLV):

$$PLV = \left| \frac{1}{n} \sum_{1}^{n} e^{i(\varphi_1 - \varphi_2)} \right|$$

which is the length of the vector average of a sample (n) of phase-differences (φ_1 - φ_2). The phase (φ) is a function of frequency and time. Being a circular mean, PLV = 1-circular variance. As such, it varies between 0 (maximum variance), when all phase-differences are uniformly distributed over 360^{o}, and 1 (minimum variance), when all phase-differences are a single value. PLV quantifies, therefore, how consistent the phase-difference is between 2 waves over a set of observations. Averaging of phase-differences can be computed over a time segment, over a sample of trials, or across several pairs of electrodes. Each of these methods has been used in the past, depending on the specific question of interest and other factors (e.g., Lachaux et al., 2000; Wang et al., 2006). Our analyses utilized the first approach: For each of the frequencies of interest, the momentary (at 1-ms resolution) phase-difference was averaged over a 500-ms time window. This analysis has the advantages of, first, utilizing a large enough sample of phase-differences, and second, preserving the trial resolution, which was useful for further computation of category selectivity (see below). The autoregressive nature of the LFP can bias the PLV: Imagine 2 perfect sinusoids simultaneously recorded over a period of time. Regardless of the size of their phase-difference, this difference will be constant and the sinusoids will appear perfectly phase-locked (PLV=1). In reality, because of multiple momentary shifts in phase/amplitude, LFPs are far from perfect sinusoids and their PLV never reaches its maximum. Still, in order to correct PLV for this bias, the trials were randomly shuffled 200 times and the average randomization PLV (i.e., the PLV expected by chance) was computed. The observed PLV was always greater than the randomization PLV, indicating that the bias was superimposed on the true synchrony between a pair of LFP signals. All PLVs we used in our analyses were bias-corrected by subtracting this bias from the observed PLV.

Synchrony was evaluated from simultaneously recorded pairs of electrodes in PFC and STR (PFC-STR, n=426), within PFC (PFC-PFC, n=240) or within STR (STR-STR, n=141). Other than PLV, the results were similar when we evaluated synchrony across trials using the standard coherence measure (e.g., Buschman et al., 2012), or pairwise phase consistency (Vinck et al., 2010). Synchrony between proximal sites (i.e., within PFC or STR) may also be vulnerable to electrotonic volume conduction. By also evaluating synchrony separately for proximal vs. distal pairs of electrodes, we confirmed that the lack of learning-induced changes in PLV within PFC and STR (Fig.3) was not due to masking by volume conduction: Neither proximal, not distal electrode pairs in PFC or STR displayed a change in synchrony across learning stages. Finally, because of the multidimensionality of a dataset like the one in this study (with dimensions like time, trials, learning stages, spectral frequency, area of recording, etc.), to increase the statistical power and computational efficiency of the analyses, it was necessary to only focus at the most critical dimensions. However, we ensured that the dimensions we chose to collapse (e.g., the trial dimension by averaging the first 16 correct trials and the time dimension by looking at 2 critical trial epochs) were inconsequential for the

results of our analyses. The results were, therefore, similar when we examined different trial epochs, or when we evaluated the evolution of synchrony across trials within a learning stage.

Similar to the LFP-LFP PLV (above) is the computation of the spike-LFP PLV:

$$PLV = \left| \frac{1}{n} \sum_{1}^{n} e^{i\varphi} \right|$$

except that n is now a sample of spike timestamps, and φ is the instantaneous frequency-specific phase at the time of each spike. This form of PLV evaluates how consistently spikes are fired at specific phase-bins of each frequency, and has two caveats: First, it is sensitive to the number of spikes, and second, it is sensitive to the temporal profile of spiking activity (see below). To partly address the former, these analyses are typically performed on multi-unit activity (MUA) instead of single-unit activity. We also did the same: we pooled all previously sorted spikes into a single MUA signal per electrode (Antzoulatos and Miller, 2011). Not only did this increase the size of spike samples, but also ensured that each electrode provided a single LFP and a single MUA signal. Another approach that is sometimes followed to address this sensitivity on spike numbers is stratification: It involves keeping the minimum number of spikes from all trials, and discarding the (randomly chosen) excess spikes. This approach was not straightforward to implement in our dataset, because the number of spikes was considerably fluctuating in the course of learning. Additionally, even stratification does not fully address the second caveat of spike-LFP PLV, which is the dependence on the temporal profile of spikes: Consider a burst of spikes occurring over a brief (say, 50-ms) time window after a visual display. Inevitably, due to their temporal clustering, these spikes will appear phase-locked at a low frequency (because at low frequencies each phase-bin lasts longer than at high frequencies). Even after stratification the spikes will most likely remain in that brief time window, thus leading to spurious PLV. Therefore, in order to correct for these biases of the MUA-LFP PLV, we randomly shuffled the trials 200 times, and subtracted the average randomization PLV, as we did for LFP-LFP PLV (above). Although this analysis did not yield evidence of general spike-LFP synchrony, evaluation of category selectivity (as described below) revealed that spike-LFP synchrony was actually category-specific (see Figs. 5 and S3).

As in our previous report of category-selective spiking activity (Antzoulatos and Miller, 2011), for category selectivity in LFP-LFP and MUA-LFP synchrony (PLV) we used the discrimination index d'. This index is calculated as the absolute difference between mean synchrony in the 2 sets of trials (category A vs. B), normalized to their pooled standard deviation s_p, i.e.,

$$d' = \frac{|\langle PLV_A \rangle - \langle PLV_B \rangle|}{s_p}$$

where

$$s_p = \sqrt{\frac{s_A^2 * (n_A - 1) + s_B^2 * (n_B - 1)}{(n_A + n_B - 2)}}$$

s^2 being the variance and n the number of each set of trials. To correct for biases generated by the variable number of trials in each category, any given set of trials was randomly shuffled between the 2 groups 200 times, thus creating a surrogate dataset. The observed d' was subsequently transformed into a z score on the basis of the surrogate data mean and variance. Similarly, we

expressed the difference between error and correct trials as a z-transformed d', except that we computed the signed (i.e., not absolute) difference of error-correct trial mean PLV (Fig.4).

Finally, our Granger causality analyses (Fig.6) relied on a nonparametric spectral matrix factorization algorithm (Dhamala et al., 2008a, 2008b), which can be found in the MATLAB-based software Fieldtrip (Oostenveld et al., 2011). Preliminary analyses with parametric Granger causality tests indicated that the optimal multivariate autoregressive (MVAR) model order (estimated using the Bayesian and Akaike criteria) was highly variable. However, because our finding that STR exerts stronger net influence on PFC was somewhat surprising (given the direct inputs from PFC to STR), we did replicate this finding using the parametric Granger test (with MVAR orders from 5 to 100) in both the time and frequency domains. These analyses were performed on the MATLAB-based software GCCA (Seth, 2010).

SUPPLEMENTAL REFERENCES:

Dhamala, M., Rangarajan, G., and Ding, M. (2008b). Estimating Granger Causality from Fourier and Wavelet Transforms of Time Series Data. Phys. Rev. Lett. *100*.

Lachaux, J.-P., Rodriguez, E., Le Van Quyen, M., Lutz, A., Martinerie, J., and Varela, F.J. (2000). Studying Single Trials of Phase Synchronous Activity in the Brain. Int. J. Bifurc. Chaos *10*, 2429–2439.

Oostenveld, R., Fries, P., Maris, E., and Schoffelen, J.-M. (2011). FieldTrip: Open Source Software for Advanced Analysis of MEG, EEG, and Invasive Electrophysiological Data. Comput. Intell. Neurosci. *2011*, 1–9.

Posner, M.I., Goldsmith, R., and Welton, K.E., Jr (1967). Perceived distance and the classification of distorted patterns. J. Exp. Psychol. *73*, 28–38.

Seth, A.K. (2010). A MATLAB toolbox for Granger causal connectivity analysis. J. Neurosci. Methods *186*, 262–273.

Vinck, M., van Wingerden, M., Womelsdorf, T., Fries, P., and Pennartz, C.M.A. (2010). The pairwise phase consistency: A bias-free measure of rhythmic neuronal synchronization. NeuroImage *51*, 112–122.

Wang, Y., Hong, B., Gao, X., and Gao, S. (2006). Phase Synchrony Measurement in Motor Cortex for Classifying Single-trial EEG during Motor Imagery. (IEEE), pp. 75–78.